J MATER RES TECHNOL. 2020;9(6):13855–13869

Available online at www.sciencedirect.com

jmr&t Journal of Materials Research and Technology

https://www.journals.elsevier.com/journal-of-materials-research-and-technology

Original Article

Enhancement of the in-plane and pin-load bearing behavior of a quasi-isotropic carbon fiber/epoxy matrix multi-scale laminate by modifying the fiber-matrix interphase using graphene nanoplatelets

Abad Arcos-Alomía[a], *Pascual Bartolo-Pérez*[b], *Alex Valadez-González*[a], *Pedro Jesus Herrera-Franco*[a,*]

[a] *Centro de Investigación Científica de Yucatán, A.C., Unidad de Materiales, Calle 43 # 130 entre 32 y 34, Col. Chuburná de Hidalgo, C.P. 97205, Mérida, Yucatán, México*

[b] *Centro de Investigación y de Estudios Avanzados del IPN, Unidad Mérida, Departamento de Física Aplicada. A.P. 73 Cordemex, 97310 Mérida, Yucatán, Mexico*

ARTICLE INFO

Article history:
Received 15 June 2020
Accepted 23 September 2020
Available online 7 October 2020

Keywords:
Graphene nanoplatelets
Carbon fiber surface properties
Bearing strength
Multiscale composites
Damage tolerance

ABSTRACT

The present work examines the effect of incorporating two different concentrations, 0.1% and 0.25%, of silane-functionalized graphene nanoplatelets GnP-GPTMS onto the carbon fiber surface of a quasi-isotropic laminate with the aim to enhance both, the laminate in-plane and the bearing strength, in a pin-loaded joint. Delamination damage modes associated with high-stress gradients were also suppressed in the in-plane loaded laminates, significantly increasing load-carrying capability. The bearing strength of a pin-loaded hole is correlated to the tensile, compression, and shear properties. The results showed an improvement of 13.8% in tensile strength for the 0.1% GnP-GPTMS concentration, as well as 17.3% for compressive strength, while for shear strength, the improvement was 11.89% for the laminate. On the other hand, the behavior of the material in the pin-loaded joint showed an increase of 10.83% for the bearing strength with the 0.1% GnP-GPTMS, fiber surface treatment. Distinct differences were noticed between the tensile stress-loaded area and the area of the residual impression of the pin in the failure mode between the only-resin treated carbon fiber composites and GnPs treated fibers. It was evident, that the interfacial shear strength (IFSS) played an important role on the failure mode. In the compression area in the pin-loaded region, there was a marked presence of a permanent deformation in the matrix. With a closer look at the local failure phenomena at the compression loaded area, there was no fiber kinking and the degree of matrix plasticity disappeared according to the level of interfacial adhesion.

* *Corresponding author.*
E-mail: pherrera@cicy.mx (P.J. Herrera-Franco).

https://doi.org/10.1016/j.jmrt.2020.09.083

1. Introduction

A known limitation of advanced composite materials is the poor strength because of the unreinforced resin-rich regions at ply interface where delamination, matrix cracking are the dominant damage modes. The ensuing issues such as damage resistance and tolerance for over-design are outstanding limitations in composite structural performance. Several approaches used to reinforce these composites in the through-thickness direction included 3D weaving, stitching, and Z-pinning [1–4]. However, because of stress concentrations that reduce the in-plane mechanical properties of the laminate, in-plane fiber movement and/or damage, fiber volume loss arising during manufacturing, use of these technologies has decreased [5].

More recently, interphase engineering of multi-scale hybrid advanced composite materials witnessed an unprecedented progress. Incorporation of nanofillers into sizing formulations was pushed forward broadly by three main reasons. First, to enhance the surface roughness of the fiber, second, to increase the local modulus of the interphase and hence, the interphase shear strength, and finally, to exploit the possible structuring of nanofillers for sensing applications [1].

The stress transfer and distribution of the carbon fiber/epoxy interfase was improved by introducing a gradient interphase reinforced by graphene oxide (GO) onto the surface of carbon fibers by physical adsorption, during the procedure of resin wetting. They found that hierarchical composites containing 0.5% (w/w) silanized GO showed a significant increase of 60% in IFSS, and 19% in interlaminar shear strength, 15% in flexural strength and 16% in flexural modulus [2]. Fang et al. [3], showed that with the addition of 0.6 % (w/w) amine-functionalized graphene nanoplatelets (GnPs), the resulting composite exhibited improvements of 93.8% in fracture toughness and 91.5% increases of flexural strength. The basic learning from all these studies was that the huge surface area of carbon nanotubes, carbon nanofibers and graphene can be exploited to enhance the specific surface area of the reinforcing fiber, provided that a covalent bond can be assured.

Carbon nanotubes have also been widely used to improve the mechanical properties of composite materials such as interlaminar shear strength, fracture toughness and, impact properties [4,6,7]. It has been shown that the efficiency of transfer of interfacial shear stresses is highly influenced by the type of fiber surface treatment used to deposit multi-walled carbon nanotubes (MWCNTs) on the surface of the carbon fiber, achieving an increase of more than 40% of IFSS when the carbon fibers were oxidized-pre-impregnated with a suitable coupling agent [8,9]. The use of graphene-related materials to modify the surface of carbon fiber fabrics has also been reported in the technical literature [10–13]. Graphene nanoplatelets have been incorporated in a matrix and different processes have been used in the manufacture of the material to improve the orientation of the graphene in the nanocomposite. When used as a coupling agent between the silicon reinforcement in an epoxy matrix at the interface, the graphene that was anchored on the surface of the silicon resulted in an increase of the elastic and flexural moduli [14,15]. Grafting of amino-functionalized graphene oxide directly onto the carbon-fiber surface by covalent bonding resulted in a 36.4% increase of the IFSS and the impact resistance of the composite material improved by 45% [16–21].

All these attempts to place either GnPs or carbon nanotubes (CNTs) onto the fiber surface, achieved through physico-chemical fiber surface modifications substantial increases of fiber-matrix interphase strength and elementary mechanical properties such as tensile, compressive, flexural and toughness. Nanoscale fibers such as CNTs have been introduced into the polymer matrix-region interphase to reinforce the laminate [22]. Other reports with CNTs and other nanomaterials have either focused solely on the interlaminar area, or the dispersion of small quantities (by volume) of unaligned CNTs within the matrix via mixing or other methods for intralaminar reinforcement. However, because of issues such as agglomeration, lack of alignment, poor dispersion, and damage to CNTs during mixing, only marginal mechanical property improvements were observed for hybrid composites when CNTs were mix into the bulk matrix [23].

Structural applications of advanced composite laminates generally use mechanical joints such as bolted and riveted joints requiring holes in the composite structure. These holes are highly susceptible to large stress concentration, which reduce the load-carrying capacity and are often responsible for unexpected composite failure. Furthermore, failure of mechanical joints in composite structures is influenced by different geometric parameters like stacking sequence, geometric parameters, ply orientation, interference fits, preloads, material properties, etc. Regarding the material properties, several researchers have used nanofillers to increase the bearing strength of the pin joints. The effect of MWCNTs content on the pin joints prepared from carbon fiber reinforced composite laminates was studied both experimentally and numerically by Kumar et al. [24]. Garcia et al. [23] grew CNTs on a Si substrate using C_2H_4/H_2 atmospheric pressure thermal chemical vapor deposition (CVD), and they transfer-printed the VACNTs to prepregs before manufacturing the composite laminate. The CNT forest maintained vertical alignment after transplantation and reported preliminary enhanced results of Mode I and II toughness tests on glass fiber reinforced composites. Using the same 3-dimensional reinforcement approach, Wicks et al. and Guzman de Villoria et al. [25,26] reinforced the z-direction with aligned CNTs at the interface between FRP plies, a region well known as a 'weak link' in laminated composites which is devoid of fiber reinforcement and fails via various modes, primarily delamination and matrix cracking. They showed that laminate in-plane strengths increased and the delamination damage modes associated with pre-ultimate failure are suppressed in the in-plane loaded laminates, significantly increasing load-carrying capability and critical strength by 30% of tension-bearing tests.

There are reports on the use of nanofillers such as Al_2O_3, nanoclay and TiO_2, which enhanced the ultimate bearing loads of the pin joints. However, none of them have examined the effect of graphene nanoplatelets on the load-bearing capacity of the fiber-reinforced composite pin joints. Additionally, the effect of graphene nanoplatelets adhesion to both the fiber surface and the matrix polymer on the pin joint performance has not been reported to the best of our knowledge [27–31].

Table 1 – Specifications of the pristine graphene oxide nanoplatelets.

Category	Diameter (μm)	Thickness (nm)	Specific surface area (g/m^2)
GnP-C750	< 2	5-7	~ 750

The state of stress in the vicinity around the pin-loaded hole is complex, especially at points located close to the boundary of the hole, where the stress components show steep gradients. There are tensile stresses in the ligament areas in the direction of the applied load, on both sides of the hole which are the regions of tensile failure; compressive stresses along the line located below the hole parallel and collinear with the vertical diameter of the hole, which is the site where bearing failures can occur; and shear stresses along the vertical lines tangent to the hole, which are the locations of shear-out failures [32–35].

In this work, the inclusion of GnPs on the fiber-matrix interphase to enhance the mechanical properties of a quasi-isotropic carbon fiber-epoxy matrix composite, especially the load-bearing properties required in a pin-loaded joint was studied. The effect of the adhesion at the fiber-matrix interphase of silane-functionalized graphene nanoplatelets GnP-GPTMS for two different concentrations, 0.1% and 0.25%, to increase the in-plane and z-direction strengths of a quasi-isotropic laminate was analyzed. The deposition of GnPs on the carbon fibers was performed using a mixture that was applied directly to the fiber prior to composite preparation. Different mechanical tests were performed to determine the properties of the material under tensile, compressive, shear, and bearing loads, as a function of GnPs content. Also, the tensile stresses in the ligament, compressive in the bearing region, and shear-out of the joint were correlated to the strength values measured in each individual loading mode.

2. Material and methods

2.1. Materials

The diglycidyl ether bisphenol A aromatic epoxy resin (DEGBA, DER331), with an equivalent epoxy weight of 182−192 g/eq, was purchased from a subsidiary of the Dow Chemical Company. The carbon fibers were acquired from Sika-Wrap model 301C unidirectional with a specific surface area of $300 \pm 15\ g/m^2$. GnP-C750 Graphene nanoplatelets were obtained from XG Sciences in Lansing, MI, E.U.A. and their specifications provided by the manufacturer are listed in Table 1. 3-glycidyl-oxypropyl-trimethoxysilane (Z6040, 236.34 g/mol), acetone and ethylenediamine (1, 2-diaminoethane, ≥ 99%, Aldrich) as a curing agent, were all from Sigma Aldrich.

2.2. Carbon fiber oxidation treatment

For the oxidation treatment of the carbon fibers a mixture of sulfuric acid/nitric acid concentrated in a ratio of 3:1 (v/v) was used together with sonication in an ultrasonic bath (Branson M8800H at 40 kHz) at 60 °C for 15 min. Then, the unidirectional fabric was removed from the ultrasonic bath and washed until the pH of the fiber was equal to that of distilled water [36]. The fibers were then dried at 100 °C for 2 h in the oven, as indicated in Fig. 1a.

2.3. Functionalization of the graphene nanoplatelets

35 mg of GnP-C750 were weighted and dispersed in 100 mL of distilled water using an ultrasonic tip at 60 W, with a 30:30 pulse ratio for 30 min. This suspension was heated to 50 °C on a heating plate and stirred continuously with a magnetic bar and 1 mL of 3-glycidyl-oxy-propyltrimethoxysilane (Z6040) was added. The recorded pH of the solution right after addition of the silane coupling agent was 5.0.The solution was heated to 70 °C and left under stirring for 12 h and filtered after that using a sintered vessel with a 0.25 μm filter. The pH was measured again and no change was noticed. The paste obtained from the filtrate was washed with 10 mL of ethanol and dried at 50 °C for one hour (see in Fig. 1b).

2.4. Composite material preparation

The unidirectional carbon fiber fabric was cut into rectangles of 27cm × 23cm in the 0°, 90°, ± 45° directions, to form a quasi-isotropic laminate $[0°, 90°, \pm 45°]_s$ with a total of 8 layers. For the deposition of functionalized graphene (GnP-GPTMS) on the unidirectional fabric, two different mixtures of acetone with GnP-GPTMS, epoxy resin and catalyst, one with 0.1 % (w/w) and the second with 0.25 % (w/w) weight percentages of GnP-GPTMS were prepared. The GnP-GPTMS were first dispersed in acetone using an ultrasonic probe for 1 h with a pulse ratio of 10: 5 s and a power of 30 W. Next, 4% (w/w) of the epoxy resin was added with continuous magnetic stirring for 10 min on a heating plate. When the resin was dissolved, the catalyst (6.9 % (w/w) with respect to the resin) was added and left for 5 min under stirring. For the deposition of the nanomaterial on the fibers, the mixture was applied to the unidirectional fiber fabric using a brush (see Fig. 1c), and the fabric was immediately dried for 150 s at 100 °C to evaporate the solvent [[20]], [37]] [38],]. A stoichiometric ratio of 100:13.8 of epoxy resin and catalyst was used for the hand lay-up manufacturing process of the laminate. The fibers were impregnated with the resin and placed in the mold followed by the peel ply, the perforated release film, the breather material and the system was closed. Vacuum was applied to the bag together with an external pressure of 74.5 kPa and kept for 2 h (see Fig. 1d). The laminate was left at room temperature for 24 h and then post cured for 2 h at 120 °C. A reference laminate without any GnP-GPTMS was prepared following the same manufacturing and curing procedure.

2.5. Fiber surface multielement analysis

Carbon fiber fabric and GnP-GPTMS were analyzed by scanning electron microscopy (SEM) and by dispersive X-ray spectroscopy (EDS) to study changes of their morphology, caused by the surface treatments and the composition. A scanning electron microscope, JSM-6360LV (JEOL USA) was also used to perform the EDS. The acceleration potential was 20 keV for the GnPs images at magnifications of 500x and 40,000 ×. For

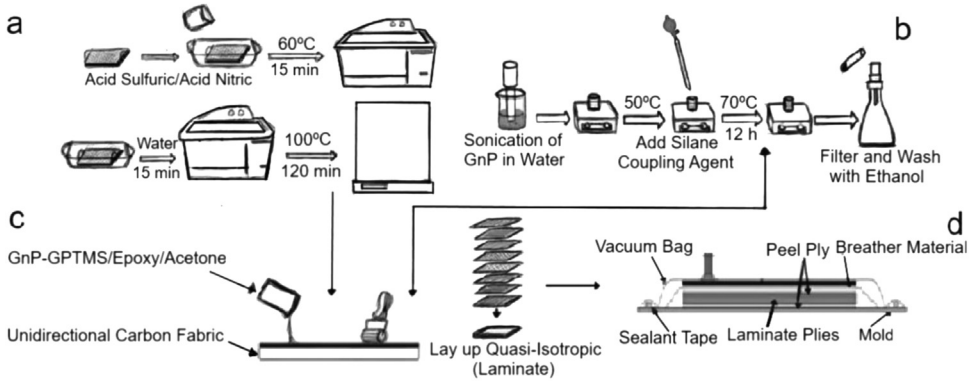

Fig. 1 – Schematic process of a) carbon fiber oxidation, b) functionalization of nPG-C750, c) incorporation of the GnP-GPTMS mixture and d) rolling.

the images of the fibers, magnifications of 10,000x and an acceleration potential of 20 keV were used.

2.6. *Infrared spectroscopy FTIR*

The FTIR analysis of the GnPs and carbon fiber samples was carried out with a Bruker FT-IR 37 spectrometer using total attenuated reflectance (ATR-FTIR) mode with 1 cm^{-1} resolution and 32 scans for both samples in the wave number range from 4000 to 400 cm^{-1}.

2.7. *Carbon fiber topography analysis*

Scanning electron microscopy (SEM) and atomic force microscopy (AFM) were used to study the morphology changes caused by the GnP-GPTMS treatments. A field emission scanning electron microscope (FE-SEM, JSM-6700 F) was used at 5 kV to observe the presence of GnPs on the carbon fiber with magnifications of 5000x and 20,000 ×. The samples were fixed on the sample holder using copper tape; no conductive coating was applied to the samples.

The roughness maximum (R_{max}) and the surface area changes resulting from the treatments of the carbon fiber surfaces were obtained using a Bruker Atomic Force Microscope (AFM), model INNOVA SPM using a tapping mode. The images were obtained at air atmosphere at ambient temperature using a cantilever beam shaped commercial silicon tip with a resonance frequency of approximately 300 KHz. This tip was the Bruker RTEST nanoprobe with a spring constant of 40 N/m and a tip radius of 8 nm. The scanning frequency of 0.5 Hz was used to scan 3μm × 3μm random areas.

2.8. *Mechanical testing*

All mechanical tests were performed on a Shimadzu Model AGS-1 Autograph universal testing machine at 25 °C using a 100 kN load cell. For the tensile and mechanical joint tests a crosshead speed of 2 mm/min was used. For the compression samples a load cell of 20 kN was used at a speed of 1.5 mm/min. For the tensile tests, 5 specimens for each type of carbon surface treatment were tested. In the case of the compression, shear and mechanical fastening tests, six specimens for each carbon surface treatment were tested. All samples were conditioned at 25 °C and a relative humidity of 50 % for 48 h prior to testing. Sample dimensions for the mechanical tests are shown in Fig. 2.

2.8.1. *Tensile test*

The tensile properties of the quasi-isotropic composite materials were determined according to the ASTM D3039 standard [39]. Strains were recorded using a 25 mm gage length extensometer and tabs were placed at the ends of the specimens.

2.8.2. *Compression test*

The compression properties were determined as indicated in the ASTM-D3410 standard using the IITRI accessory [40]. Tabs made of phenolic plates were placed on the specimens to prevent buckling of the sample and to ensure that failure of the material occurred in the calibration length.

2.8.3. *Shear test*

The shear tests were performed using the Iosipescu accessory according to ASTM-D5379 [41]. The specimens were cut using a vertical milling machine with a prismatic milling cutter. Tabs were placed at the ends of the specimens to strengthen and stabilize the sample by increasing the thickness locally in the grip region, thus minimizing local bearing failures in the grip region of the accessory and to reduce the possibility of torsion of the specimen.

2.8.4. *Pin-loaded joint strength*

This experiment allows assessing the effect of the inclusion of the GnPs in the enhancement of the joints and their failure modes under tensile loads that can usually occur in four different basic modes, namely, due to tearing, tensile failure in the effective net section, shear failure and bearing failure. In particular, for a sufficient end distance e and width w in joint laminates, there is generally a dominant failure mode consisting of a local compression laminate failure induced by the tendency of the pin to crush the composite material, with local occurrence of cracks in the matrix [3]. Bearing failure is characterized by high compressive stress values within the zone surrounding the loaded inner hole boundary, and it is a gradual and progressive failure mode of non-catastrophic nature

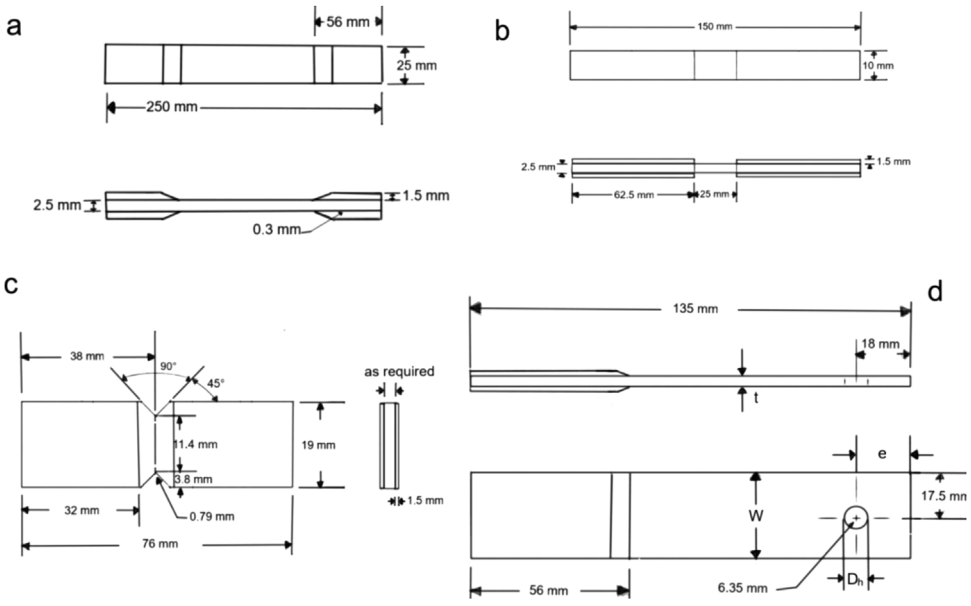

Fig. 2 – Dimensions of the specimens a) tensile test, b) compression test, c) Iosipescu shear test, and d) pin-loaded specimen.

[25]. The bearing test was performed according to procedure A of the ASTM-D5961 standard [42]. The bearing strength σ_b was calculated using the following equation:

$$\sigma_b = P/D_h t \quad (1)$$

Where D_h is the diameter of the hole, t is the thickness of the specimen and P is the force applied to the specimen. The tensile stress in the ligament area σ_{tl} of the specimen was estimated using the following equation:

$$\sigma_{tl} = P/(W\text{-}D_h)t \quad (2)$$

Here W is the width of the specimen. The shear-out stress was estimated using the following equation:

$$\tau_{out} = P/2et \quad (3)$$

Where e is the longitudinal distance from the center of the hole to the end edge of the sample (see Fig. 2d)

2.9. *Acoustic Emission Monitoring of tensile test and bearing strength*

Two piezoelectric transducers were used to monitor the acoustic emissions (AE). The distance between these transducers was set at 70 mm apart on the tensile test specimens. For the joint tests, the transducers were set at 15 mm apart on the ligament area, that is, on the tensile stress loaded area around the hole; to ensure good contact between the transducers and the material, vacuum silicon grease was used. A threshold of 30 dB generally used in most fiber-reinforced composites was set to observe the AEs [43,44]. The AE were processed using the Micro 11 PCI-2 acoustic emission system. The wave velocity for each formulation of composite material was obtained by the Hsu-Nielsen technique consisting on breaking a pencil graphite tip over the tested sample; this test indirectly calculates the velocity of acoustic wave propagation through the specimen material. When recording AE in the tensile tests, the composite material samples were not loaded to failure.

3. Results and discussion

3.1. *ATR-FTIR for GnP and carbon fiber*

Fig. 3a shows the FTIR spectra of both, pristine and silanized GnPs and the functional groups can be observed qualitatively. Comparing the spectra of graphene and silanized nanoplatelets, the appearance and loss of bands in the FTIR spectrum indicate the presence of silane on the graphene structure. The presence of the band 3483 cm^{-1} denotes the appearance of the –OH stretching bond, the band at 1767 cm^{-1} shows the existence of the group C=O stretching bond, the peak 1594 cm^{-1} indicates the stretching bond of the C=C group. This is a characteristic sp^2 signal since the manufacturing processes of these nanoplatelets are non-oxidative. The peak in 1240 cm^{-1} denotes the torsion bond of the -C–OH group [19,38]. In the spectrum of the silanized graphene, the appearance of two peaks at 2956 cm^{-1} and 2874 cm^{-1}, (stretching) and at 775 cm^{-1} (rocking) suggests the presence of the $-CH_2$ group [45,46]. Also, the carbonyl group C=O characteristic peaks at 1747 cm^{-1} and 1594 cm^{-1} [47] and of the SiO group at 1136 cm^{-1} and 917 cm^{-1} [44,45] can be appreciated.

Fig. 3b shows the spectrum of the pristine and oxidized carbon fibers, the pristine fiber shows a broad peak at 3068 cm^{-1} representing the stretching of the CH group of the epoxy rings, the peak at 1531 cm^{-1} and 1281 cm^{-1} show the presence of the CO group respectively in flexion and stretching, and the 1115 cm^1 peak shows the double C=C bond due to the epoxy [47,48]. For the oxidized fiber, the band 3068 cm^{-1} has to disappear while the presence of the peak in 2913 cm^{-1} of the CH group is observed. The

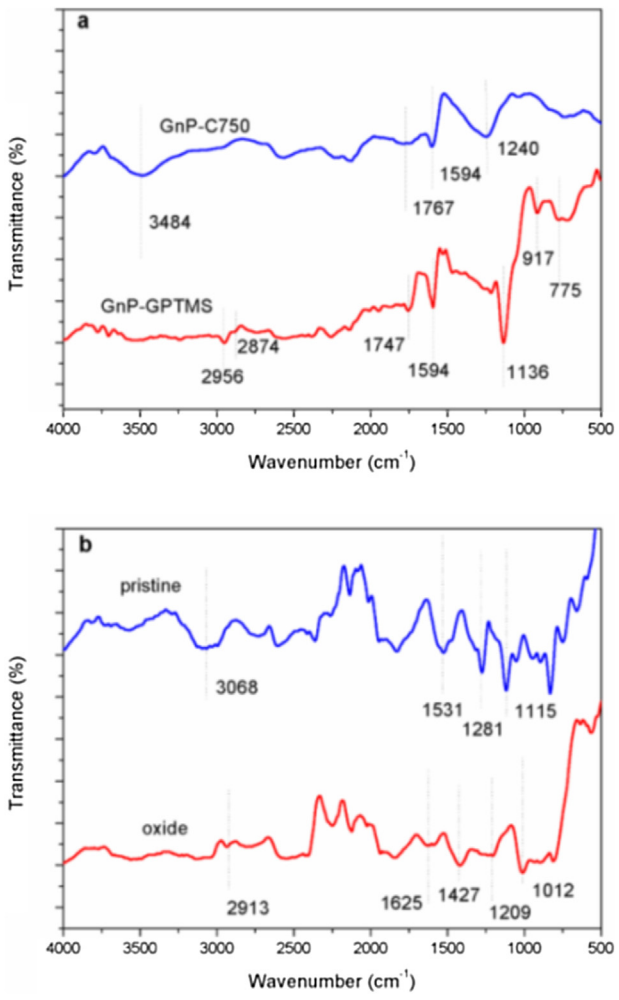

Fig. 3 – FTIR spectra of a) graphene nanoplates and b) carbon fiber.

appearance of peaks in 1625 cm^{-1}, 1427 cm^{-1} and 1209 cm^{-1} show the presence of the C=O ketone group with stretching and torsion movements in the fiber due to oxidation, finally the peak in 1012 cm^{-1} is the bending of the aromatic C=C bond [45,49].

3.2. *SEM for GnP and carbon fiber*

Scanning electron microscopy (SEM) images are shown in Fig. 4 for pristine and silanized GnPs nanoplatelets, Fig. 4a shows the pristine nanoplatelets and Fig. 4b, the GnPs treated with the 3-glycidoxypropylmethoxysilane. Both pictures show agglomerations of the nanoparticles and this is attributed to the strong π-π bond present in its stacking resulting from its large surface area [36], although for the silanized graphene nanoplatelets, larger agglomerations forming more compact structures as shown in the micrographs. This may be attributed to the surface treatment. The inherent roughness of the pristine carbon fiber can be observed in Fig. 4c, while the oxidized fiber (Fig. 4d) shows greater roughness because of the treatment, without serious damages affecting its mechanical properties [49].

3.3. *EDS for GnPs and carbon fiber*

Table 2 shows data of the elements present on the graphene nanoplatelets and the carbon fibers obtained using EDS. The pristine graphene nanoplatelets contain oxygen that corresponds to the sizing applied by the manufacturer. The increase of the amount of oxygen on the oxidized fibers [37] generates new functional groups as shown in the FTIR spectra. The appearance of the silane from the treatment of the graphene nanoplatelets is confirmed.

3.4. *SEM and AFM of carbon fiber coating*

Fig. 5a shows some resin agglomerations in the resin-coated carbon fiber, while the Fig. 5b shows the image of the fiber treated with 0.1% of GnP-GPTMS where it the no-uniformly distributed nanoparticles present on its surface can be seen, but no resin agglomerations can be distinguished. Fig. 5c shows fibers with the 0.25% GnP-GPTMS concentration and a greater amount of the nanoparticles is observed but there are some agglomerates on the fiber surface which may be attributed to the increase in the viscosity of the resin because of a higher concentration of nPG-GPTMS in the coating.

Notorious differences of morphologies were also observed on the samples surfaces as seen from AFM images. Fig. 6a, which corresponds to resin-coated carbon fiber samples, exhibited smoother area than those corresponding to 0.1% of GnP-GPTMS and 0.25% of GnP-GPTMS, presented in Fig. 6b and c. Similar observations to the images obtained from SEM images can be made. The presence of agglomerates on the fiber surface did not contribute to the betterment of the mechanical properties. The RMS-surface roughness estimate from the AFM images are shown in Table 3.

A notorious change of the fiber surface area values because of the surface treatments can be appreciated, and this difference is larger for 0.1% of GnP-GPTMS. The increase in surface area means that there exists more interfacial area, that is, more sites of fiber matrix interaction, either mechanical interaction like friction and/or physico-chemical interactions resulting from the coupling agent and resin interactions [1,22,23]. Furthermore, the maximum roughness R_{max} observed for 0.25% of GnP-GPTMS, may be attributed to the presence of large agglomerates, as shown in Figs. 5c and 6c.

3.5. *In-plane mechanical properties and acoustic emission analysis*

3.5.1. *Tensile properties*

The tensile tests results for the different GnP-GPTMS percentages are shown in Fig. 7 and specimens containing 0.1% GnP-GPTMS have a higher maximum tensile strength. It can be noted that the laminates containing nanoplatelets show a significant maximum strength increase of approximately 13.8% and 10% respectively, as compared to the one that does not contain graphene nanoplatelets. Even when the tensile properties are fiber dominated, this increase is greater for the concentration of 0.1%, and it is attributed to a better distribution of the nanoplatelets around the fiber interphase, and an increase of interphase area, thus achieving a more efficient load transfer. In the case of the 0.25% of GnP-GPTMS, having

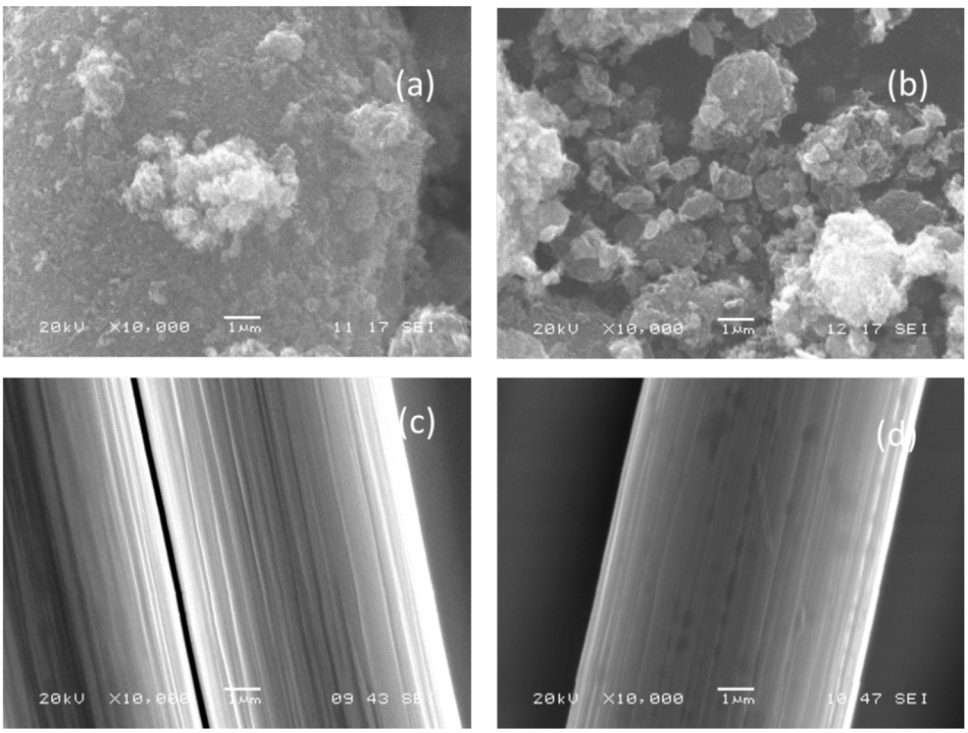

Fig. 4 – SEM images of a) GnP-C750, b) GnP-GPTMS, c) pristine carbon fiber and d) oxidized carbon fiber.

Table 2 – EDS values for the different materials.

Sample	Mass % of chemical elements			
	C	O	Si	O/C
Pristine carbon fiber	89.56(±1.51)	10.44(±1.56)	------	0.08(±0.017)
Oxidized carbon fiber	77.52(±0.76)	22.36(±0.76)	------	0.31(±0.013)
GnP-C750	87.93(±1.15)	12.15(±1.22)	------	0.14(±0.015)
GnP-GPTMS	75.14(±1.26)	19.89(±2.72)	4.8(±1.25)	0.27(±0.037)

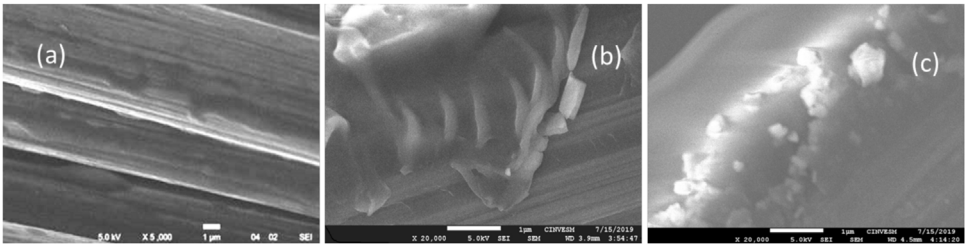

Fig. 5 – Micrograph images a) resin-coated fiber, b) 0.1% of GnP-GPTMS, c) 0.25% of GnP-GPTMS.

Table 3 – Surface area and Roughness of carbon fibers specimens: a) Resin-coated fiber, b) with 0.1% of GnP-GPTMS and c) with 0.25% of GnP-GPTMS.

Carbon fiber treatment	Surface area (μm^2)	Projected Surface area (μm^2)	Surface area difference (%)	Roughness R_{max} (nm)
Resin-coated fiber	0.0938	0.0936	0.277	3.8
0.1% of GnP-GPTMS	0.0965	0.0936	3.09	11.8
0.25% of GnP-GPTMS	0.0944	0.0936	0.939	30.4

higher graphene content in the interphase region, can lead to agglomerations that resulted in a reduction of interphase area, thereby reducing the stress transfer from the fiber to the matrix. In addition, the vacuum content is slightly higher and this may lead to a weak interphase that can lead to friction between the fibers [38] as shown in SEM images of the fiber coating. The elastic modulus of the composite material with 0.25% of GnP-GPTMS shows an increase of 26.7% and the one

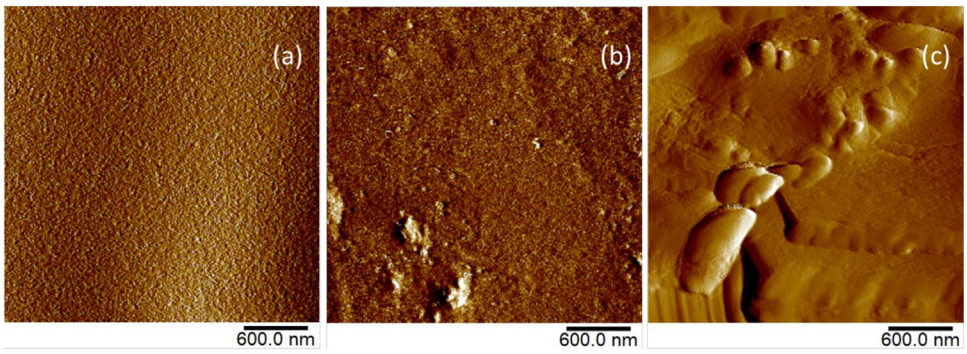

Fig. 6 – AFM topography of: a) resin-coated fiber, b) 0.1% of GnP-GPTMS, c) 0.25% of GnP-GPTMS.

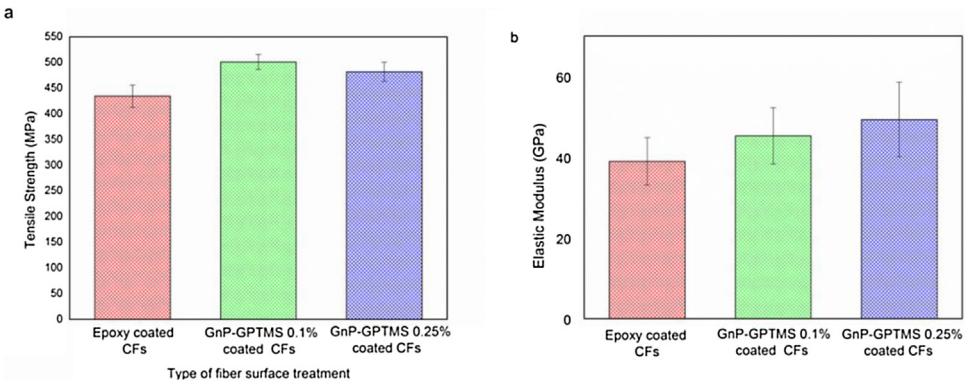

Fig. 7 – Tensile properties for laminates with different fiber surface treatments: a) tensile strength and b) elastic modulus.

that contains 0.1% shows an increase of 16.3% as compared to the one that does not contain the nanoplatelets. However, even when the 0.25% of GnP-GPTMS composite showed a higher maximum tensile strength value, its modulus of toughness, u_t, of was approximately 15% higher those for 0.1% of GnP-GPTMS or resin only composites. Similar results were reported by Kamar et al. about the ability of graphene nanoplatelets (GnPs) to improve the interlaminar mechanical properties of glass-reinforced multilayer composites with the addition of only 0.25 wt% GnP [21].

Fig. 8 shows the tensile test results and the associated acoustic emission events. A great number of them can be noticed for the laminate with carbon fibers without GnPs (Fig. 8a), most of them in the range of amplitudes of 35-60 dB, which are usually attributed to failure of the matrix material in the acoustic spectrum. As observed in Fig. 8d, three histograms show the amplitude and the number of acoustic emission events. Both, amplitude and number of events are greater for the laminate that does not contain GnPs followed by those with 0.25% and 0.10% of GnP-GPTMS [43].

These results are consistent with those obtained from the values of maximum strength and elastic modulus since lower AE events, i.e., less noise, indicate a better stress transfer between the fiber and the matrix, thereby increasing the properties of the composite material that contains GnPs.

Fig. 9 shows images of the fracture surfaces of specimens loaded in tension for the composite material and the different carbon fiber surface treatments. Fig. 9a, shows the resin only treated fiber and that some resin traces remain on their surface, indicating that there is good adhesion. It can be inferred that failure of the composite material is more interfacial than cohesive. Fig. 9b corresponds to the composite material coated with 0.1% of GnP-GPTMS where a larger amount of resin is noted between the fibers indicating a better interfacial adhesion. Fig. 9c shows the fracture surface of the specimen with the coating with 0.25% of GnP-GPTMS. A greater presence of resin on the fibers is noticed but there are also areas where the fibers debonded off the matrix, indicating some interfacial failure and more cohesive failure. All these observations are in good agreement with the results obtained by means of AE and the observations made with both the SEM and AFM analysis.

3.5.2. *Compression properties*

As shown in Fig. 10, the specimens containing 0.1% of silanized graphene nanoplatelets, higher compression strength of 165.0 MPa is observed, while those that do not contain any graphene and the one with 0.25% silanized graphene nanoplatelets have compression strengths of 141.0 MPa and 152.0 MPa respectively. Then, the compressive strength increased approximately 17.0%, and 7.8 % because of the incorporation of 0.1% of GnP-GPTMS and 0.25% of GnP-GPTMS respectively in the fiber-matrix interphase. This behavior may be attributed to the lateral support resulting from the presence of graphene at the interphase, that is, the GnPs acted as a support around the fiber, thus preventing fiber failure by buckling or shear, allowing a better load to be transferred more effectively. For the 0.25% of GnP-GPTMS, although it contains a greater amount of GnP, the poor distribution did not it

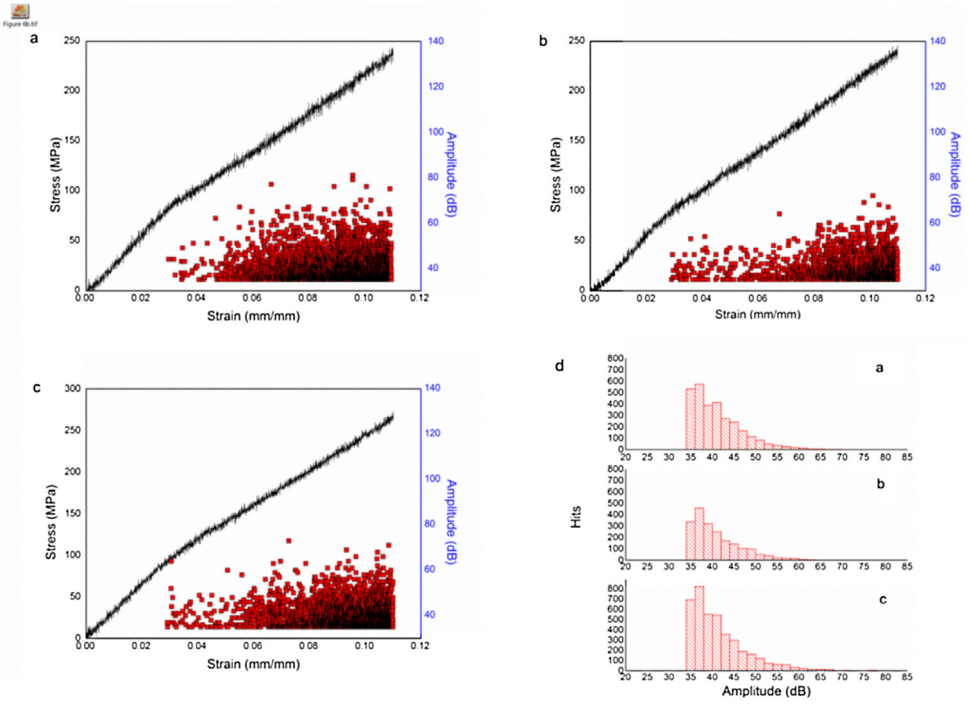

Fig. 8 – Stress-strain graph for tensile stress test associated with acoustic emission events a) for lamination without GnP-GPTMS, b) laminated with 0.1% of GnP-GPTMS, c) laminated with 0.25% of GnP-GPTMS and d) Histogram of the amplitude in relation to the number of events for each type of laminate mentioned in a-c.

Table 4 – Mechanical pin-loaded Joint testing summary data.

Specimen type	Tensile strength/Tensile joint stress ratio σ_0/σ_{tl}	Shear strength/Shear-out joint stress ratio τ_0/τ_{out}	Compressive strength/Bearing stress ratio σ_c/σ^{br}	Bearing chord stiffness, E^{br} (GPa)
Resin-only untreated fiber	$\frac{435.0}{37.0} = 11.8$	$\frac{122}{73} = 1.67$	$\frac{141}{167} = 0.85$	1.48
0.1% of GnP-GPTMS	$\frac{501}{38} = 13$	$\frac{141}{75.5} = 1.85$	$\frac{165}{186} = 0.89$	1.90 (30.2% +)
0.25% of GnP-GPTMS	$\frac{482}{37} = 13$	$\frac{125}{73} = 1.70$	$\frac{152}{185} = 0.82$	2.70 (83.3% +)

allow an efficient lateral support that results in a less efficient load transfer between fibers and the matrix, and perhaps also resulting in the generation of stress concentrators in the material. The strain to failure values are higher in the laminate that does not contain the nanoparticle while for those with higher GnP content, it decreased.

3.5.3. *Shear properties*

Fig. 11 shows the force-displacement graph of the shear test characteristic in this type of test, showing the highest values obtained for each of the treatments. The graph shows a higher displacement for the sample containing 0.1% of GnP and has a higher value of load at failure, showing that the content of the GnP does have an influence on the shear behavior of the composite material. It can be inferred from the shape of the graphs that when the load reaches a maximum value the composite material with untreated fibers fails and the load suddenly drops. In the case of the GnP treated carbon fibers, a shoulder that differs depending on the GnP content is noticed. Those samples containing graphene have a wider shoulder. This behavior may be because of the two dimensions of graphene results in a better response to shear stresses and failure is not catastrophic. The maximum shear strength values are 69.0 ± 2.0 MPa, 78.0 ± 2.0 MPa and 70.0 ± 4.0 MPa for untreated fibers, 0.1% and 0.25% GnP-GPTMS respectively, obtaining increases of 13.0% and 1.0% for 0.1% and 0.25% GnP-GPTMS as compared to the untreated fiber.

3.5.4. *Bearing pin-loaded joint response*

Fig. 12 shows the tensile stress in the net cross section, the bearing compressive stress and the shear-out stress plot for the mechanically fastened pin-loaded joint test. It can be seen in Fig. 12a that the interfacial modifications resulting from the introduction of GnP onto the carbon fiber surface have no noticeable effect on the tensile behavior of the loaded joint. It can be considered that the tensile strength is a fiber-dominated behavior of the composite material, especially the 0° oriented plies, aligned with the load. The bearing strength for the different formulations, calculated taking the highest values of applied load from the test are shown in Fig. 12b. In this case, it should be remembered that the laminates used are $[0°, 90°, \pm 45°]_S$ quasi-isotropic and that this type of laminate typically fails because of bearing stresses in the hole section. It should also be remembered that in this test, the coupons are subjected to a complex state of stress in the vicinity of the hole.

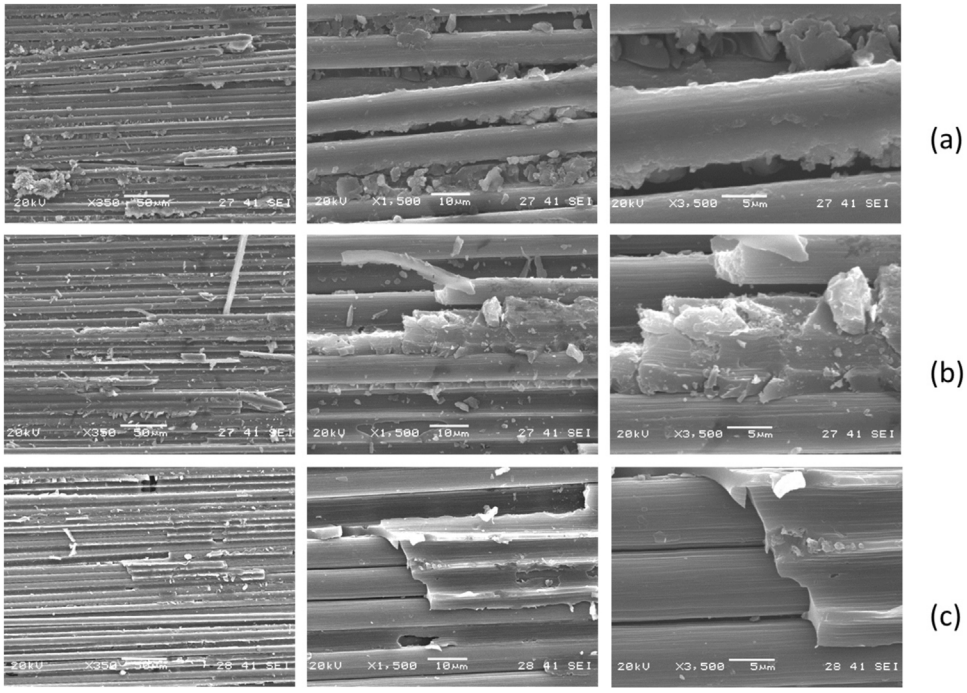

Fig. 9 – SEM images of the tensile test fracture surfaces for specimens: a) without GnP, b) with 0.1% of GnP-GPTMS and c) with 0.25% of GnP-GPTMS.

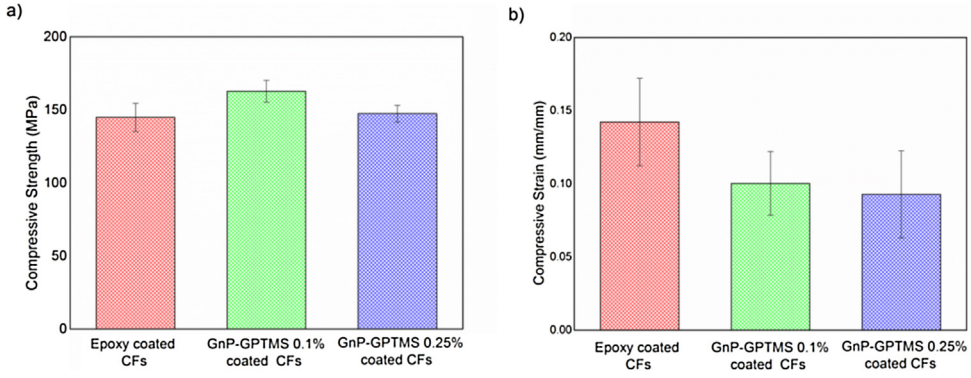

Fig. 10 – Compression properties for laminates with different fiber surface treatments a) compressive strength and b) compressive strain.

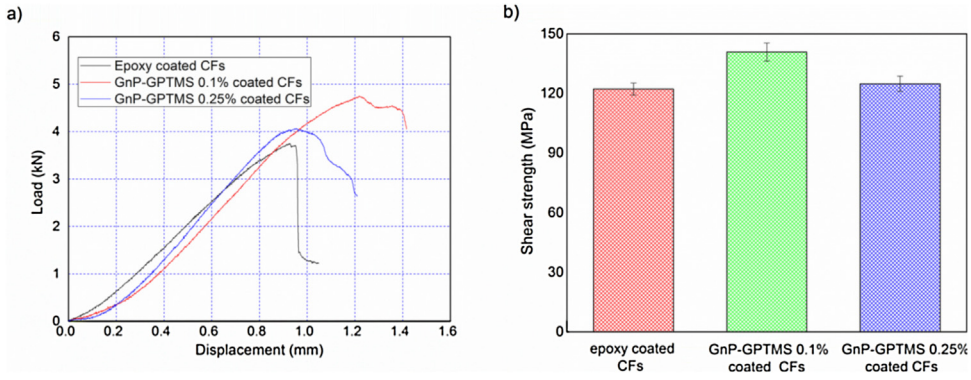

Fig. 11 – Iosipescu shear test results for laminates with different fiber surface treatments: a) shear load-displacement and b) shear strength for the different carbon fiber surface treatments.

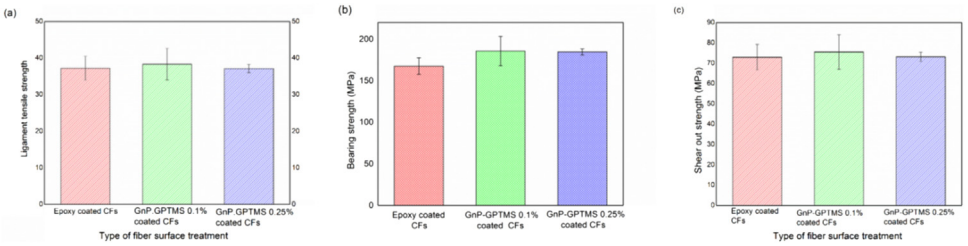

Fig. 12 – Test results for pin-loaded joint for laminates with three different fiber surface treatments: a) tensile stresses in the net tensile section; b) bearing strength in the area of contact between the joint and the pin; c) shear-out stresses.

There exists a high gradient of tensile stress component in the ligament sections on both edges of the hole, the compressive stress in the pin-laminate contact region and shear stresses in between these regions. The bearing failure is characterized by high compressive stress values within the zone surrounding the loaded inner hole boundary and it is a gradual and progressive failure mode of non-catastrophic nature. The tensile stress in the net-cross sectional area, for each of the three formulations was: 37.0 ± 3.0 MPa, 38.0 ± 4.0 MPa and 37.0 ± 1.2 MPa, for the only resin, 0.1% and 0.25% GnP-GPTMS fiber treatments respectively. As mentioned before, the tensile behavior is a fiber-dominated property and the carbon fiber surface modification only allowed a slightly larger deformation before failure. Similar results were observed for the shear-out strength and their values were: 73.0 ± 6.0 MPa, 75.5 ± 8.5 MPa, and 73.0 ± 2.0 MPa, for the only resin, 0.1% and 0.25% of GnP-GPTMS samples respectively. The largest increase was approximately 3.5% for the 0.1% GnP-GPTMS fiber surface treatment.

The bearing strength values were 167.5 ± 10.0 MPa, 186.0 ± 18.0 MPa and 185.0 ± 4.0 MPa for only resin, 0.1% and 0.25% GnP-GPTMS respectively. The 0.1% GnP-GPTMS formulation increased 11.0% while the 0.25% GnP-GPTMS, 10.0%, as compared to the resin only one. It is evident that the presence of the GnPs plays a very important role in the behavior of the composite material, especially when subjected to a complex state of stress. As mentioned before, the joint strength has a dependency on the addition of nanomaterials like MWCNT in different compositions. Additionally, the tensile strength of the MWCNT added carbon/epoxy composite laminates increases with increase in MWCNT composition up to 0.3 wt.% [24].

The bearing chord stiffness, E^{br}, was calculated from the bearing stress/bearing strain plot when recording the AEs (Fig. 14). The bearing chord stiffness is calculated between two specific bearing stress or bearing strain points corresponding to the linear portion of the curve using the relation: $E^{br} = \Delta\sigma^{br}/\Delta\varepsilon^{br}$, where $\Delta\sigma^{br}$ and $\Delta\varepsilon^{br}$ are the changes in the bearing stress and the bearing strain over the chord stiffness range, respectively. In this case, the hole deformation was normalized by the hole diameter to estimate an effective bearing strain. Likewise, the applied force was normalized by the projected hole area to estimate an effective bearing stress. It is convenient to point out that the bearing chord stiffness was recorded together with the acoustic emission signals. That is, the specimen was not loaded until a maximum failure force had clearly been reached. The test was terminated earlier to prevent masking of the true failure mode by large-scale hole distortion in order to provide a more representative failure mode assessment.

Instead of using a specific failure criterion for the progressive damage analysis of the pin-loaded joint, simple strength ratios (SR) for tensile, shear and compressive loads versus the estimated stress components for the joint are shown in Table 4. Again, it can be seen that the Tensile strength /Tensile joint stress ratio (SR), σ_0/σ_{tl} is much larger than 1, and this is attributed to the 0° fibers aligned in the load direction. Then for the lamination stacking sequence selected for this experiment, a tensile failure is far from occurring. In the case of the shear strength (Iosipescu shear strength) /shear-out stress ratio $\tau_0/\tau_{out} > 1.0$, the largest value is occurring for the 0.1% GnP-GPTMS carbon fiber surface treatment. The axial compression strength and the bearing strength σ^{br}, yields a ratio of 165.23 /185.66 equal to 0.89, closer to 1.0 unlike the resin only treatment or the 0.25% GnP-GPTMS. The Bearing chord stiffness, E^{br} is noticed to increase with increasing GnP content. From Fig. 15, the areas under the curves for the resin-only, 0.1% GnP-GPTMS and the 0.25% GnP-GPTMS and the strain energies were 1.1, 1.5 and 3.6 MJ/m^3 respectively. However, the ultimate failure of the 0.25% GnP-GPTMS was lower than that observed for the 0.1% GnP-GPTMS. This may be attributed to a poorer distribution of the GnPs at higher volume fractions.

The SEM images of Fig. 13a show that the fibers with resin-only coating suffered extensive interfacial failure with the debonding of the fiber from the matrix. These images correspond to points in the transition from the bearing area where a crushing failure may occur and points subjected to tensile stresses in the ligament in the vicinity of the hole. A distinct difference is noticed between the tensile stress-loaded area and the area of the residual impression of the pin on the only resin treated carbon fiber composites and GnPs treated ones. It was evident, that the IFSS played an important role on the failure mode. In the compression area there is a marked presence of a permanent deformation in the matrix. A closer look at the local failure phenomena in the compression loaded area, the degree of matrix plasticity appears to vary according to the level of interfacial adhesion. In Fig. 13b for 0.1% of GnP-GPTMS a greater amount of resin is adhered to the fiber which speaks of a cohesive failure on the matrix, while for Fig. 13c for the 0.25% GnP-GPTMS, small tufts of deformed epoxy around the fiber ends can also be distinguished in the tensile loaded regions. Also, for Fig. 13b and c, in the pin-loaded area only a few fiber failures by buckling or shear are noticed in the bear-

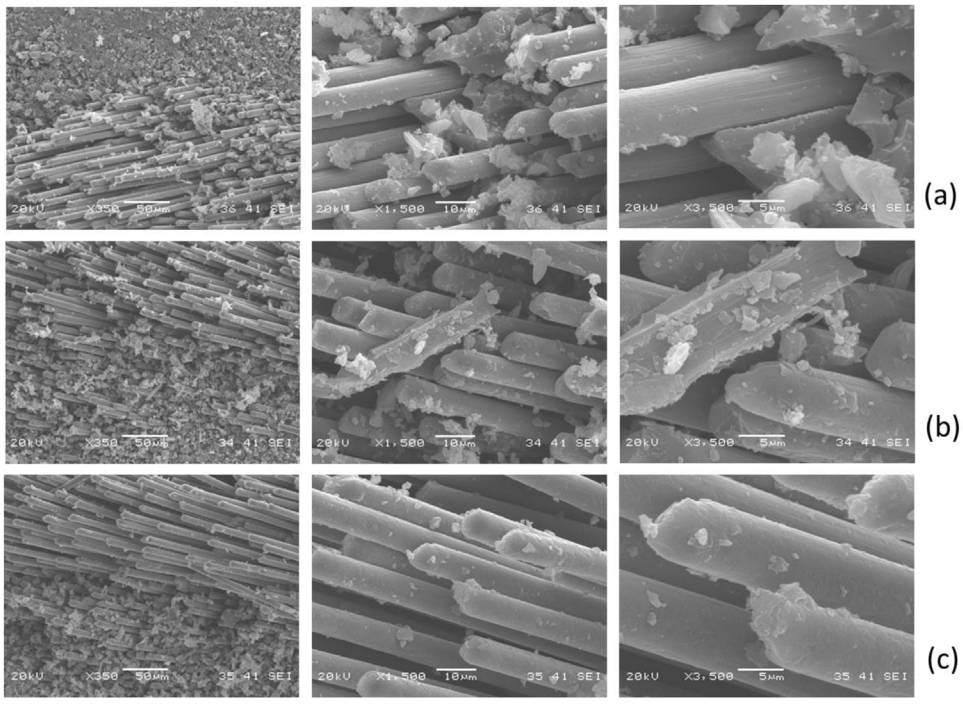

Fig. 13 – SEM images of the fracture surface in the mechanical joint specimens corresponding to points located in the transition zone between the bearing stress and the tensile stress in the ligament regions for: a) resin-only coating, b) 0.1% of GnP-GTMPS and c) 0.25% of GnP-GTMPS, at different magnifications.

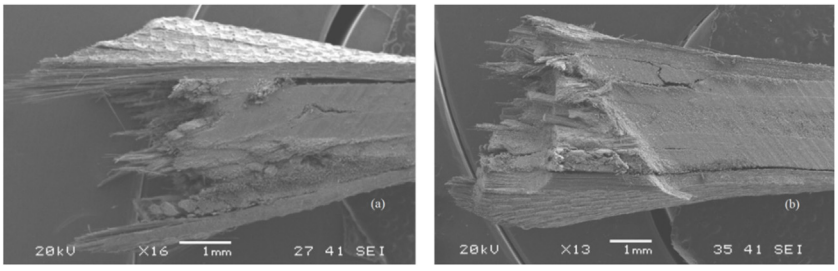

Fig. 14 – Pin-loaded hole specimen after failure to show bulging at the hole edge and delamination between the 0°/90° plies for: (a) a) resin only, b) with 0.1% of GnP-GTMPS.

ing region in the transition to tensile failure. It is postulated that the appearance of abraded region is caused by buckling of fibers as a result of the geometry of the pin which tends to bow the fiber ends inward, however, the presence of the GnPs tends to prevent fiber buckling. This may also be related to any frictional forces which are present between the composite surface and the pin. These characteristic modes of deformation were consistently observed for both systems with GnP. Kamae and Drzal, [50] stated that because of the inclusion of CNTs on the fiber surface, one of the properties of the composite laminate, expected to be improved is the compressive strength in the fiber direction because the shear modulus and shear strength of a matrix resin would be enhanced by preventing fiber buckling. Furthermore, the presence of GnPs on the fiber-matrix interphase besides increasing the in-plane stiffness of the laminate also provides additional through-thickness stiffness, both of which are important in resisting bearing failure. Similar observations were made by Wicks et al. [25] who used aligned CNTs to increase the in-plane stiffness of the laminate and to provide additional through-thickness stiffness.

Visual evidence of z-direction (through-thickness) stiffness enhancement is shown by the laminate cross-sections after failure in Fig. 14. The resin only specimen expands (“bulging of the bearing joint”) in the through-thickness direction near the hole, in the region of bearing failure, for the 0.1% of GnP-GPTMS composite was of approximately a 38% of the initial thickness and as compared to a 44% of the resin only composite. Delamination, especially between the 0°/90° plies was also less notorious because of the z-direction enhancement of the GnPs.

The AE events recorded close to the hole are shown in Fig. 15. The resin-only coating sample showed a greater number of AE with respect to the one that contains 0.1% of GnP-GPTMS, in addition to the fact that most of the AE were in the range of 30-50 dB, indicating matrix failure in the composite material. It could also be noticed that these AE events corresponding to the resin-only samples started at lower bear-

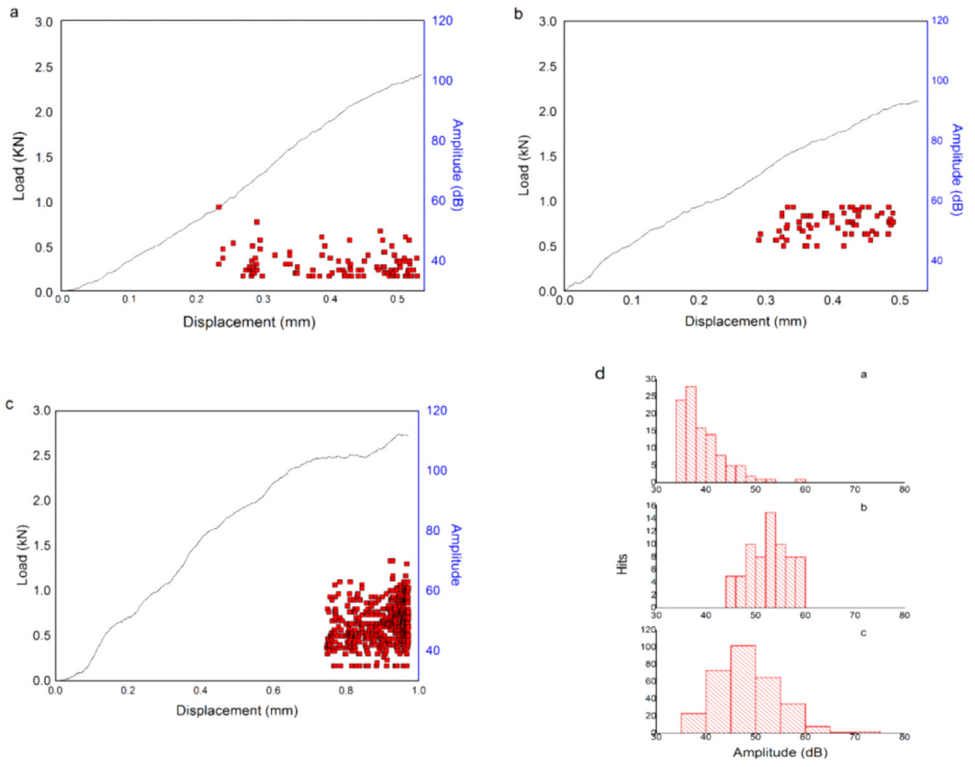

Fig. 15 – Bearing Stress-Bearing Strain graph associated with acoustic emission events: a) for laminate without GnP-GPTMS, b) laminate with 0.1% of GnP-GPTMS, c) laminate with 0.25% of GnP-GPTMS and d) histogram of the acoustic events amplitude versus the number of events for each type of laminate according.

ing strain values, long before the acoustic events occur in samples containing 0.1% GnP-GPTMS. In this case, most of the AE events occur in the range of 40–60 dB, indicating matrix and fiber failure of the material but with fewer AE events than those observed for the resin-only samples. For the 0.25% of GnP-GPTMS samples, more AE events than those recorded for the other two fiber surface conditions, but In this case, they occur at a higher bearing strain and most of these AE events were in a range of 30–70 dB. Again, this may also be related to any frictional forces which are present between the composite surface and the pin in addition to the matrix and fiber failure.

4. Conclusions

The benefit of the deposition of the GnP-GPTMS on the carbon fiber-epoxy resin matrix interphase proved to increase the interfacial surface area, resulting in an improvement of the mechanical behavior of a quasi-isotropic laminate. Two different GnP-GPTMS concentrations were studied and the best results were obtained with a 0.1% concentration. For higher GnP-GPTMS contents, no noticeable strength value increases were observed. Tensile tests on the material with 0.1% GnP-GPTMS, showed an increase of 13.8% with respect to the untreated fiber, while the deformation in the three formulations did not show significant changes. The elastic modulus increased in the material with 0.25% graphene by approximately 26.7% when compared with the untreated CFs. In the Iosipescu shear test, the increase in the shear strength of 11.89% for the 0.1% for silanized GnPs with respect to the untreated one was observed. The strength behavior of pin-loaded joint, showed similar results to the single-mode load tests. The benefit of the deposition of the GnP-GPTMS on the fiber surface was more notorious on the in-plane strength, specially the bearing strength of the composite material. An increase of 10.83% with respect to the laminate with untreated fibers was estimated. The strength ratios (SR) increased because of the adhesion of the GnPs to the fiber. The z-direction behavior (through the thickness direction) was also enhanced and smaller z-direction displacements were notice at the hole/pin contact edge. Delamination between the 0° and 90° plies was less notorious. Distinct differences were noticed between the tensile stress-loaded area and the area of the bearing strength produced in the area of contact between the pin and the laminate. The residual impression of the pin on the failure mode between the only-resin treated carbon fiber composites showed a marked degree of matrix plastic deformation for untreated fibers. As the IFSS increased with the inclusion of the GnPs, such plastic matrix deformation decreased, thus indicating that the fibers did not failed under compression and/or fiber buckling and shear. It was evident that the IFSS played an important role in the in-plane and z-direction failure mode.

Conflict of interest

The authors declare no conflicts of interest.

Acknowledgements

The authors would like to thank Javier Cauich-Cupul, for training Mr. Arcos-Alomía in the use of mechanical testing equipment. Thanks are given to María Verónica Moreno-Chulim for help with the AFM images. This study was funded by Consejo Nacional de Ciencia y Tecnología of México, CONACYT (Grant CB-2012-01.183418 and Infrastructure Grant 253762) and also a scholarship granted to Mr. Abad Arcos-Alomía is highly appreciated. All four authors declare that they have no conflict of interest.

REFERENCES

[1] Karger-Kocsis J, Mahmood H, Pegoretti A. Recent advances in fiber/matrix interphase engineering for polymer composites. Prog Mater Sci 2015;73:1–43, http://dx.doi.org/10.1016/j.pmatsci.2015.02.003.

[2] Chen L, Jin H, Xu Z, Shan M, Tian X, Yang C, et al. A design of gradient interphase reinforced by silanized graphene oxide and its effect on carbon fiber/epoxy interface. Mater Chem Phys 2014;145:186–96, http://dx.doi.org/10.1016/j.matchemphys.2014.02.001.

[3] Fang M, Zhang Z, Li J, Zhang H, Lu H, Yang Y. Constructing hierarchically structured interphases for strong and tough epoxy nanocomposites by amine-rich graphene surfaces. J Mater Chem 2010;20:9635–43, http://dx.doi.org/10.1039/C0JM01620A.

[4] Bekyarova E, Thostenson ET, Kim YH, Gao J, Tang J, Hahn HT, Chou TW, Itkis ME, Haddon RC. Multiscale carbon nanotube-carbon Fiber reinforcement for advanced epoxy composites. Langmuir 2007;23(7):3970–4, http://dx.doi.org/10.1021/la062743p.

[5] Tong L, Mouritz AP, Bannister M. 3D fibre reinforced polymer composites. Oxford: Elsevier; 2002.

[6] Godara A, Mezzo L, Luizi F, Warrier A, Lomov SV, van Vuure AW, et al. Influence of carbon nanotube reinforcement on the processing and the mechanical behaviour of carbon fiber/epoxy composites. Carbon 2009;47:2914–23, http://dx.doi.org/10.1016/j.carbon.2009.06.039.

[7] Ashrafi B, Guan J, Mirjalili V, Zhang Y, Chun L, Pl Hubert, et al. Enhancement of mechanical performance of epoxy/carbon fiber laminate composites using single-walled carbon nanotubes. Comp Sci and Technol 2011;71(13):1569–78, http://dx.doi.org/10.1016/j.compscitech.2011.06.015.

[8] Muñoz-Vélez MF, Valadez-González A, Herrera-Franco PJ. Effect of fiber surface treatment on the incorporation of carbon nanotubes and on the micromechanical properties of a single-carbon fiber-epoxy matrix composite. Express Polym Lett 2017;11:704–18, http://dx.doi.org/10.3144/expresspolymlett.2017.68.

[9] Herrera-Sosa ML, Valadez-González A, Vázquez-Torres H, Mani-González PG, Herrera-Franco PJ. Effect of the surface modification using MWCNTs with different L/D by two different methods of deposition on the IFSS of single carbon fiber-epoxy resin composite. Carbon Lett 2017;24:18–27, http://dx.doi.org/10.5714/CL.2017.24.018.

[10] Hung P-Y, Lau KT, Fox B, Hameed N, Lee JH, Hui D. Surface modification of carbon fibre using graphene–related materials for multifunctional composites. Compos Part B: Eng 2018;133:240–57, http://dx.doi.org/10.1016/j.compositesb.2017.09.010.

[11] He P, Huang B, Liu L, Huang Q, Chen T. Preparation of multiscale graphene oxide-carbon fabric and its effect on mechanical properties of hierarchical epoxy resin composite. Polym Compos 2016;37:1515–22, http://dx.doi.org/10.1002/pc.23321.

[12] Pathaka AK, Borah M, Gupta A, Yokozeki T, Dhakate SR. Improved mechanical properties of carbon fiber/graphene oxide-epoxy hybrid composites. Comp Sci and Technol 2016;135:28–38, http://dx.doi.org/10.1016/j.compscitech.2016.09.007.

[13] Deka BK, Hazarika A, Kong K, Kim D, Park YB, Park HW. Interfacial resistive heating and mechanical properties of graphene oxide assisted CuO nanoparticles in woven carbon fiber/polyester composite. Compos Part A-Appl Sci Manuf 2016;80:159–70, http://dx.doi.org/10.1016/j.compositesa.2015.10.023.

[14] Wu H, Drzal LT. Graphene nanoplatelet-polyetherimide composites: revealed morphology and relation to properties. J Appl Polym Sci 2013;130:4081–9, http://dx.doi.org/10.1002/app.39678.

[15] Chen L, Chai S, Liu K, Ning N, Gao J, Liu Q, Chen F, Fu Q. Enhanced Epoxy/Silica composites mechanical properties by introducing graphene oxide to the interface. ACS Appl Mater Interfaces 2012;4(8):4398–404, http://dx.doi.org/10.1021/am3010576.

[16] Zhang RL, Gao B, Ma QH, Zhang J, Cui HZ, Liu L. Directly grafting graphene oxide onto carbon fiber and the effect on the mechanical properties of carbon fiber composites. Mater Des 2016;93:364–9, http://dx.doi.org/10.1016/j.matdes.2016.01.003.

[17] Ning H, Li J, Hu N, Yan C, Liu Y, Wu L, et al. Interlaminar mechanical properties of carbon fiber reinforced plastic laminates modified with graphene oxide interleaf. Carbon 2015;91:224–33, http://dx.doi.org/10.1016/j.carbon.2015.04.054.

[18] Jiang D, Liu L, Wu G, Zhang Q, Long J, Wu Z, et al. Mechanical properties of carbon fiber composites modified with graphene oxide in the interphase. Polym Compos 2017;38:2425–32, http://dx.doi.org/10.1002/pc.23828.

[19] Wang F, Drzal LT, Qin Y, Huang Z. Size effect of graphene nanoplatelets on the morphology and mechanical behavior of glass fiber/epoxy composites. J Mater Sci 2016;51:3337–48, http://dx.doi.org/10.1007/s10853-015-9649-x.

[20] Qin W, Vautard F, Drzal LT, Yu J. Mechanical and electrical properties of carbon fiber composites with incorporation of graphene nanoplatelets at the fiber–matrix interphase. Compos Part B Eng 2015;69:335–41, http://dx.doi.org/10.1016/j.compositesb.2014.10.014.

[21] Kamar NT, Hossain MM, Khomenko A, Haq M, Drzal LT, Loos A. Interlaminar reinforcement of glass fiber/epoxy composites with graphene nanoplatelets. Compos Part A Appl Sci Manuf 2015;70:82–92, http://dx.doi.org/10.1016/j.compositesa.2014.12.010.

[22] Mei L, Li Y, Wang R, Ch Wang, Peng Q, He X. Multiscale carbon nanotube-carbon Fiber reinforcement for advanced epoxy composites with high interfacial strength. Polymers & Polymer Composites 2011;19(2 & 3):107–12, http://dx.doi.org/10.1177/0967391111019002-309.

[23] Garcia EJ, Wardle BL, Hart AJ. Joining prepreg composite interfaces with aligned carbon nanotubes. Compos Part A Appl Sci Manuf 2008;39:1065–70, http://dx.doi.org/10.1016/j.compositesa.2008.03.011.

[24] Kumar M, Saini JS, Bhunia H. Investigations on the strength of mechanical joints prepared from carbon fiber laminates with addition of carbon nanotubes. J Mech Sci Technol 2020;34(3):1059–70, http://dx.doi.org/10.1007/s12206-020-0208-2.

[25] Wicks SS, Guzman de Villoria R, Wardle BL. Interlaminar and intralaminar reinforcement of composite laminates with

aligned carbon nanotubes. Compos Sci Technol 2010;70:20–8, http://dx.doi.org/10.1016/j.compscitech.2009.09.001.
[26] Guzman de Villoria R, Hallander P, Ydrefors L, Nordin P, Wardle BL. In-plane strength enhancement of laminated composites via aligned carbon nanotube interlaminar reinforcement. Comp Sci and Technol 2016;133:33–9, http://dx.doi.org/10.1016/j.compscitech.2016.07.006.
[27] Asi O. An experimental study on the bearing strength behavior of Al2O3 particle filled glass fiber reinforced epoxy composites pinned joints. Compos Struct 2010;92:354–63, http://dx.doi.org/10.1016/j.compstruct.2009.08.014.
[28] Atar M, Ahmadpour SM, Banisadr SS, Mohammadi A, Mirmoradi SZ, Shirazi Z. The effect of Al2O3 nano additions on failure of GFRP plate with two parallel pin loaded holes. J Mech Sci Technol 2019;3:2769–76, http://dx.doi.org/10.1007/s12206-019-0523-7.
[29] Singh M, Saini JS, Bhunia H. Investigation on failure modes for pin joints made from unidirectional glass–epoxy nanoclay laminates. Fatigue & Fracture of Enginering Materials & Structures 2016;39:320–34, http://dx.doi.org/10.1111/ffe.12358.
[30] Sekhon M, Saini JS, Singla G, Bhunia H. Influence of nanoparticle fillers content on the bearing strength behavior of glass fiber-reinforced epoxy composites pin joints. Proc Inst Mech Eng Part L J Mater Des Appl 2017;231:641–56, http://dx.doi.org/10.1177/1464420715607556.
[31] Singh K, Saini JS, Bhunia H, Singh J. Investigations to increase the failure load for joints in glass epoxy composites. Proceedings of the Institution of Mechanical Engineers, Part C: Journal of Mechanical Engineering Science 2019 2019;233:2074–90, http://dx.doi.org/10.1177/0954406218779617.
[32] Herrera Franco PJ, Cloud GL. Strain-relief inserts for composite fasteners - an experimental study. J. Compos Mats 1994;26:751–68, http://dx.doi.org/10.1177/002199839202600506.
[33] Khashaba UA, Sebaey TA, Mahmoud FF, Selmy AI, Hamouda RM. Experimental and numerical analysis of pinned-joints composite laminates: effects of stacking sequences. J. of Compos Mats 2013;47:1–14, http://dx.doi.org/10.1177/0021998312464891, 3353-3366.
[34] Pisano AA, Fuschi P. Mechanically fastened joints in composite laminates: evaluation of load bearing capacity. Compos Part B Eng 2011;42:949–61, http://dx.doi.org/10.1016/j.compositesb.2010.12.016.
[35] Thoppul SD, Finegan J, Gibson RF. Mechanics of mechanically fastened joints in polymer–matrix composite structures – a review. Compos Sci Technol 2009;69:301–29, http://dx.doi.org/10.1016/j.compscitech.2008.09.037.
[36] Zhang G, Sun S, Yang D, Dodelet J-P, Sacher E. The surface analytical characterization of carbon fibers functionalized by H2SO4/HNO3 treatment. Carbon 2008;46:196–205, http://dx.doi.org/10.1016/j.carbon.2007.11.002.
[37] Fukushima H, Jurek R, Drzal LT. Carbon Fiber/Graphite nano platelet hybrid composites. In: Proceedings of ICCM-17. Edinburgh. 2009. UK July.
[38] Marcano DC, Kosynkin DV, Berlin JM, Sinitskii A, Sun Z, Slesarev A, et al. Improved synthesis of graphene oxide. ACS Nano 2010;4:4806–14, http://dx.doi.org/10.1021/nn1006368.
[39] ASTM D3039, Standard Test Method for Tensile Properties of Polymer Matrix Composite Materials, American Society for Testing and Materials, 100 Barr Harbor Drive, PO Box C700, West Conshohocken, PA 19428-2959. United States of America.
[40] ASTM D3410/D3410M, Standard Test Method for Compressive Properties of Polymer Matrix Composite Materials with Unsupported Gage Section by Shear Loading, American Society for Testing and Materials, 100 Barr Harbor Drive, PO Box C700, West Conshohocken, PA 19428-2959. United States of America.
[41] ASTM D5379/D5379M-19, Standard Test Method for Shear Properties of Composite Materials by the V-Notched Beam Method, American Society for Testing and Materials, 100 Barr Harbor Drive, PO Box C700, West Conshohocken, PA 19428-2959. United States of America.
[42] ASTM D5961/D5961M-17, Standard Test Method for Bearing Response of Polymer Matrix Composite Laminates, American Society for Testing and Materials, 100 Barr Harbor Drive, PO Box C700, West Conshohocken, PA 19428-2959. United States of America.
[43] Marec A, Thomas J-H, Guerjouma RE. Damage characterization of polymer-based composite materials: multivariable analysis and wavelet transform for clustering acoustic emission data. Mech Syst Signal Process 2008;22:1441–64, http://dx.doi.org/10.1016/j.ymssp.2007.11.02.
[44] Barré S, Benzeggagh ML. On the use of Acoustic Emission to investigate damage mechanisms in glass-fibre-reinforced polypropyle. Compos Sci Technol 1994;52:369–76, http://dx.doi.org/10.1016/0266-3538(94)90171-6.
[45] Yang H, Li F, Shan C, Han D, Zhang Q, Niu L, Ivaska A. Covalent functionalization of chemically converted graphene sheets via silane and its reinforcement. J of Mate Chem 2009;19:4632–8, http://dx.doi.org/10.1039/B901421G.
[46] Hou S, Su S, Kasner ML, Shah P, Patel K, Madaran CJ. Formation of highly stable dispersions of silane-functionalized reduced graphene oxide. Chem Phys Lett 2010;501:68–74, http://dx.doi.org/10.1016/j.cplett.2010.10.051.
[47] Dai Z, Shi F, Zhang B, Li M, Zhang Z. Effect of sizing on carbon fiber surface properties and fibers/epoxy interfacial adhesion. Appl Surf Sci 2011;257:6980–5, http://dx.doi.org/10.1016/j.apsusc.2011.03.047.
[48] Silverstein RM, Bassler GC. Spectrometric identification of organic compounds. J Chem Educ 1992;39:546, http://dx.doi.org/10.1021/ed039p546.
[49] Moreno-Castilla C, Lopez-Ramon MV, Carrasco-Marin F. Changes in surface chemistry of activated carbons by wet oxidation. Carbon 2000;38:1995–2001, http://dx.doi.org/10.1016/S0008-6223(00)00048-8.
[50] Kamae T, Drzal LT. Carbon fiber/epoxy composite property enhancement through incorporation of carbon nanotubes at the fiber–matrix interphase – part I: the development of carbon nanotube coated carbon fibers and the evaluation of their adhesion. Compos Part A Appl Sci Manuf 2012;43:1569–77, http://dx.doi.org/10.1016/j.compositesa.2012.02.016.